



# One-step synthesis of highly reduced graphene hydrogels for high power supercapacitor applications

Harish Banda, David Aradilla, Anass A Benayad, Yves Chenavier, Barbara Daffos, Lionel Dubois, Florence Duclairoir

## ► To cite this version:

Harish Banda, David Aradilla, Anass A Benayad, Yves Chenavier, Barbara Daffos, et al.. One-step synthesis of highly reduced graphene hydrogels for high power supercapacitor applications. Journal of Power Sources, 2017, 360, pp.538-547. 10.1016/j.jpowsour.2017.06.033 . hal-02025387

**HAL Id: hal-02025387**

**<https://hal.science/hal-02025387>**

Submitted on 26 Feb 2019

**HAL** is a multi-disciplinary open access archive for the deposit and dissemination of scientific research documents, whether they are published or not. The documents may come from teaching and research institutions in France or abroad, or from public or private research centers.

L'archive ouverte pluridisciplinaire **HAL**, est destinée au dépôt et à la diffusion de documents scientifiques de niveau recherche, publiés ou non, émanant des établissements d'enseignement et de recherche français ou étrangers, des laboratoires publics ou privés.




## Open Archive Toulouse Archive Ouverte (OATAO)

OATAO is an open access repository that collects the work of Toulouse researchers and makes it freely available over the web where possible

This is an author's version published in: <http://oatao.univ-toulouse.fr/21805>

**Official URL:** <https://doi.org/10.1016/j.jpowsour.2017.06.033>

### **To cite this version:**

Banda, Harish and Aradilla, David and Benayad, Anass and Chenavier, Yves and Daffos, Barbara  and Dubois, Lionel and Duclairoir, Florence *One-step synthesis of highly reduced graphene hydrogels for high power supercapacitor applications*. (2017) Journal of Power Sources, 360. 538-547. ISSN 0378-7753

Any correspondence concerning this service should be sent  
to the repository administrator: [tech-oatao@listes-diff.inp-toulouse.fr](mailto:tech-oatao@listes-diff.inp-toulouse.fr)

# One-step synthesis of highly reduced graphene hydrogels for high power supercapacitor applications

Harish Banda <sup>a</sup>, David Aradilla <sup>a,\*</sup>, Anass Benayad <sup>b</sup>, Yves Chenavier <sup>a</sup>, Barbara Daffos <sup>c,d</sup>, Lionel Dubois <sup>a</sup>, Florence Duclairoir <sup>a,\*\*</sup>

<sup>a</sup> Univ. Grenoble Alpes, CEA, CNRS, INAC, SyMMES, F-38000 Grenoble, France

<sup>b</sup> Univ. Grenoble Alpes, CEA, LITEN, F-38000 Grenoble, France

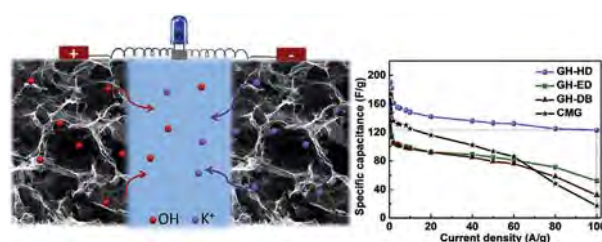
<sup>c</sup> CIRIMAT, Université de Toulouse, CNRS, INPT, UPS, 118 Route de Narbonne, 31062 Toulouse, cedex 9, France

<sup>d</sup> Réseau sur le Stockage Electrochimique de l'Energie (RS2E), FR CNRS, 3459, France

## HIGHLIGHTS

- Highly reduced graphene hydrogels for high performance supercapacitor applications.
- Hydrazine-based graphene hydrogels exhibits an excellent SC of 123 Fg<sup>-1</sup> at 100 Ag<sup>-1</sup>
- High power and energy density compared to literature with an excellent stability.

## GRAPHICAL ABSTRACT



## ARTICLE INFO

### Keywords:

Supercapacitors  
Graphene hydrogels  
Aqueous electrolyte

## ABSTRACT

Graphene hydrogels with high electrical conductivity were prepared by a one-step process using hydrazine hydrate as gel assembly agent (GH-HD). Conventional two-step process of gel formation and further reduction to prepare highly conducting gels was replaced by a single step involving equivalent amount of hydrazine. Optimized graphene oxide concentration was established to facilitate such monolith formation. Extensive characterization and control studies enabled understanding of the material properties and gel formation mechanism. The synthesized gel shows a high electrical conductivity of 1141 S/m. The supercapacitor based on GH-HD delivers a high specific capacitance of 190 F/g at a current density of 0.5 A/g and 123 F/g at very high current density of 100 A/g. Furthermore, excellent power capability and cyclic stability were also observed. 3D macroporous morphology of GH-HD makes it ideal for high rate supercapacitor applications.

## 1. Introduction

Supercapacitors (SCs) based on electrochemical double layer capacitance have attracted great interest as electrochemical energy

\* Corresponding author.

\*\* Corresponding author.

E-mail addresses: [david.aradilla@cea.fr](mailto:david.aradilla@cea.fr) (D. Aradilla), [florence.duclairoir@cea.fr](mailto:florence.duclairoir@cea.fr) (F. Duclairoir).

storage devices in the last decade [1,2]. Successful elaboration of SCs promise a wide range of applications in electric vehicles, memory back-up devices and large industrial equipment. While high power capability and long cycle-life of SC have been the driving force for this extensive scientific research, inferior energy densities compared to batteries has been a major shortcoming [3,4]. Considerable efforts on materials design have been made in attaining superior energy densities without compromising the power capability and cycle-life [5]. Graphene, a one-atom thick

layer of graphite, is among the various carbonaceous materials that are under study for this type of electrochemical storage. Graphene with its high electrical conductivity, mechanical flexibility and remarkable theoretical surface area of  $2630 \text{ m}^2/\text{g}$  is an ideal candidate for SC [6]. It is noteworthy that theoretically a high gravimetric capacitance of  $550 \text{ F/g}$  could be obtained if both surfaces of graphene were used for charge storage [7]. While synthesis of pristine graphene for practical applications is challenging, Ruoff et al. have pioneered the bulk synthesis of chemically modified graphene (CMG) as a graphene-like material [8,9]. This synthesis pathway is based on the oxidation of graphite powder to exfoliated graphene oxide (GO) that is subsequently reduced into reduced graphene oxide (rGO) - more generally described as CMG [8]. When tested in SC, CMG demonstrated good power capability in both aqueous and organic electrolytes [10]. However, low specific capacitances of 130 and 99 F/g respectively were achieved owing to limited exposition of graphene sheets to the electrolyte. This unexpectedly lower accessible surface area was explained by the restacking of individual hydrophobic graphene sheets due to strong  $\pi$ - $\pi$  interactions [10].

Later, Shi et al. have first developed self-assembled graphene hydrogels (GHs) from aqueous graphene oxide (GO) solutions [11–13]. This assembly is achieved through careful modulation of the hydrophobic/hydrophilic balances in the GO solution through either non-covalent or covalent interactions [14–22]. Two interesting monolith assembly methods are the hydrothermal treatment of a graphene oxide solution, and the bridging of graphene oxide sheets by reaction with diamine [12,23–26]. The first method can be considered as non-covalently based as the monolith formation is triggered by the GO sheets reduction under supercritical conditions followed by their physical cross-linking [12]. The second method concerns the reactivity of the terminal amines of an organic diamine structuring agent with the oxygen functionalities on the graphene oxide sheets [25]. The amine groups react with the electropositive carbons on graphene oxide and a covalent C-N bond is thus formed. Each diamine molecule could react twice and can thus bridge two graphene sheets together. In this method, the concomitant reducing nature of the diamine also plays a role in the monolith formation [25]. The covalent bond formation and the reduction of GO occur at a varied degree depending on the diamine used. It was shown that the assembly of 2D sheets into 3D monolith limits restacking of the layers, creates a unique macro porous network with pore diameters ranging from sub-micrometres to several micrometres that enables unobstructed transport of the electrolyte, and yield a 3D percolating network [17]. Hence, these GHs have been tested in SC systems and indeed showed excellent electrochemical performances [27].

In the case of the hydrothermally synthesized GH, discharge capacitance of  $200 \text{ F/g}$  is achieved at a low current density of  $0.3 \text{ A/g}$  with good cycle-life [12]. However, a great decrease in specific capacitance is observed upon increasing the current densities due to low conductivity and extensive residual oxygenated groups. Nevertheless, a subsequent hydrazine-reduction of this gel allowed reaching better capacitances at high current densities ( $222 \text{ s F/g}$  at  $1 \text{ A/g}$ ) [28]. Similar enhancement in power performances is also reported with hydrazine treatment of ethylenediamine assisted GHs. These examples from literature emphasize that an additional reduction step of the monolith is essential to achieve the highest SC performances explained by a higher electrical conductivity of the percolating network [23–25,28,29].

Interestingly, depending on the reducing agent nature and reaction parameters, chemical reduction of GO in itself has been identified as an efficient gel assembly method. For example, reducing agents such as ascorbic acid,  $\text{NaHSO}_3$ ,  $\text{Na}_2\text{S}$  and HI were proposed as assembly initiators to form high conducting gels in

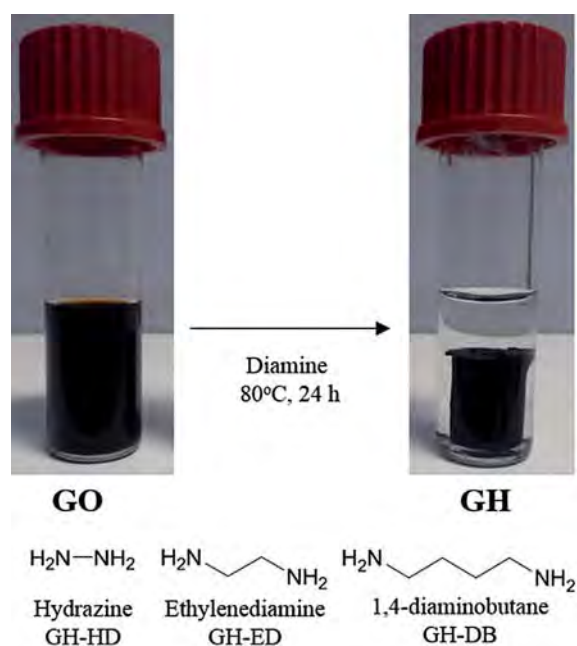
varying shapes [30]. Surprisingly, hydrazine hydrate, an excellent reducing agent, which originally instigated the development of CMG and was also used to further reduce the assembled gels, was shown to be ineffective for monolith assembly under specific conditions [30]. Yan et al. have suggested that the presence of residual nitrogen in the gel may prevent monolith formation with hydrazine [30]. However, now it is well known that nitrogen doped gels are indeed possible [23–26]. Hence, successful demonstration of a monolith using hydrazine is conceivable and promises an excellent conducting GH for high power supercapacitors.

Herein, we demonstrate that the graphene monolith assembly using hydrazine monohydrate is indeed feasible. A simple one-step synthesis process under optimized reaction conditions enables exceptionally conducting gels (GH-HD) with excellent power capabilities. Furthermore, instead of large quantities of hydrazine monohydrate as reported earlier, a molar equivalent of reagent corresponding to GO is used. For comparison and better understanding of the mechanisms involved, GH with other longer chain diamines such as ethylenediamine (GH-ED) and 1,4-diaminobutane (GH-DB) have also been synthesized (Scheme 1). The synthesized GH-HD demonstrates a high capacitance of  $190 \text{ F/g}$  at a current density of  $0.5 \text{ A/g}$  and a remarkable cyclic stability over 2000 cycles at  $10 \text{ A/g}$ . Moreover, a high capacitance of  $123 \text{ F/g}$  could be retained at a very high current density of  $100 \text{ A/g}$ . Although gravimetric capacitances were conventionally used as the evaluation criterion of a SC, volumetric capacitance is considered to be a crucial measure for portable applications with limited space [31–36]. By adapting a simple drying technique [31], we could double the volumetric capacitance of  $110 \text{ F/cm}^3$  for freeze dried GH-HD to  $257 \text{ F/cm}^3$  at  $0.5 \text{ A/g}$ .

## 2. Experimental

### 2.1. Synthesis of graphene hydrogels

An aqueous solution of well dispersed  $5 \text{ mg/ml}$  GO was prepared as a precursor for the synthesis of various GHs. GO synthesis was achieved through a modified-Hummers and Offeman's method as



**Scheme 1.** Schematic of the gel formation process with different diamines used.

reported previously [37]. Details of the reaction procedures and filtration techniques are given in the supplementary information (SI). Prior to the synthesis, 15 ml of 5 mg/ml GO solution and 5.7 mmol of diamine were sonicated in a sealed vial for 10 min. The vials were then heated in an oil bath at 80 °C for 24 h under no stirring condition. GH-HD, GH-ED and GH-DB were obtained by addition of 5.7 mmol of hydrazine monohydrate (0.28 ml), ethylenediamine (0.38 ml) and 1, 4-diaminobutane (0.5 g) respectively. The obtained gels were washed with copious amounts of water to remove any unreacted diamine. Freeze drying was performed at −37 °C to obtain dried GHs with preserved 3D structures for characterization. A dense GH-HD was obtained by air-drying the hydrogel (GH-HD-AD) for 48 h and then heated under vacuum at 60 °C overnight.

## 2.2. Fabrication of supercapacitors

The as prepared cylindrical GHs were cut into several slices of GH (~1 mm thickness). In order to find out the exact mass, a calibration of the dried mass to wet mass of the slices was established by freeze drying some of the cut pieces. Two slices of wet gels with same mass were chosen and pressed onto nickel foams under 10 MPa pressure. A piece of filter paper (Whatman filter paper) was used as a separator between the electrodes. Electrodes and filter paper, soaked overnight in 6 M KOH electrolyte, were assembled as a layered structure into a home-made Swagelok-type two electrode cell configuration with stainless steel as current collector. Similarly, three electrode measurements were performed in 6 M KOH using a home-made three electrode experimental set-up with Pt wire as counter and Calomel electrode as reference.

## 2.3. Electrochemical measurements

The performance of SC were evaluated using cyclic voltammetry (CV), galvanostatic charge-discharge (GCD) cycles and electrochemical impedance spectroscopy (EIS). A multichannel VMP3 potentiostat/galvanostat with EC-Lab software (Biologic) was used for all electrochemical techniques. CV and charge-discharge measurements in two electrode set-up were performed between 0 and 1 V with scan rates from 10 mV/s to 1000 mV/s and 0.5 A/g to 100 A/g respectively. CVs were obtained at 10 and 100 mV/s in a three electrode configuration in the voltage range of −0.9 V to 0.1 V. Graphene hydrogels were used as working electrode, platinum foil as counter electrode and calomel as reference electrode. EIS tests were performed with a frequency range between 400 kHz and 40 mHz and AC perturbation of 10 mV. The gravimetric capacitances ( $C_{wt}$ ) of GHs derived from galvanostatic discharge curves were calculated by using the equation  $C_{wt} = 2I/(m(\Delta V/\Delta t))$ , where  $I$  is the constant discharge current,  $m$  is the mass of one electrode and  $\Delta V$  and  $\Delta t$  represent voltage change (excluding  $V_{drop}$ ) on discharge and time for full discharge respectively. The corresponding volumetric capacitances ( $C_{vol}$ ) were calculated as follows:  $C_{vol} = C_{wt} \times \rho$ , where  $\rho$  is the packing density of GH. The gravimetric energy and power densities were calculated as  $E_{wt} = C_{wt}V^2/8$  and  $P = E_{wt}/\Delta t$ . Packing densities were obtained by calculating the mass of the dried gel with a precision of 0.01 mg and by measuring the dimensions using scanning electron microscopy.

## 2.4. Characterization techniques

A Mettler-Toledo XPE205 weighing balance was used to obtain weights of the samples with a precision of 0.01 mg. The changes in the chemical bonding were analyzed by Fourier transformed infrared spectroscopy (FT-IR, Thermofischer ES 50) in the frequency range of 4000–400  $\text{cm}^{-1}$ . The materials were tested using KBr

pellets. The crystallographic structures of the materials were determined by a wide-angle X-ray diffraction (XRD) system on a Panalytical X'pert PRO X-ray diffractometer using a Co K $\alpha$  radiation source ( $\lambda = 1.79 \text{ \AA}$ ). The thermogravimetric analysis (TGA) of all samples were performed with Setaram TGA 92 at a heating ramp rate of 5 °C/min from 30 °C to 800 °C under nitrogen atmosphere. Electrical conductivity values were obtained using a four-probe measurement technique. Thin films prepared by pressing a cut piece of gel under 10 MPa were used for these measurements. Packing densities were also calculated by measuring mass and volume of these films. X-ray photoelectron spectroscopy (XPS) analyses were performed using a PHI Versa Probe II spectrometer with a monochromatized Al K $\alpha$  X-ray source (1486.6 eV) focalized to a spot of 100  $\mu\text{m}$  and with an electron take-off angle of  $\theta = 45^\circ$ . Survey spectra of the photo-emitted electrons were recorded with a pass energy of 117 eV and the high-resolution spectra with a pass energy of 23.5 eV. The deconvolution of C 1s and N 1s core-level spectra was performed by fitting the individual components at values obtained from earlier reports by using Casa XPS software [25,29]. Spectra were fitted into Gaussian-Lorentzian (30) shaped curves with full width at half maximum values kept under 1.5 in all cases. The morphology of the GH materials was characterized using a Zeiss Ultra 55 electron microscope at an accelerating voltage of 7 kV. Methylene blue adsorption method was used to determine the solvated surface area. The detailed protocol is described in the ESI. Porosity characteristics were calculated from nitrogen sorption isotherms measured at 77 K with Micromeritics ASAP 3020 porosimeter. Prior to the analysis samples have been subjected to a degazing at 100 °C for 24 h. The specific surface area was estimated using both Brunauer–Emmett–Teller (BET) and density functional theory (DFT) method while the pore volumes and the pore size distributions (PSD) were calculated from adsorption isotherms by using quenched solid density functional theory (QSDFT) method.

## 3. Results and discussion

In this study, the graphene monolith assembly is obtained by reacting GO solution with a diamine structuring agent at 80 °C for 24 h under no stirring condition (Scheme 1). Concentration of the GO solution and molar equivalents of the diamine used are two important parameters in the gel formation. An earlier report describing the effort to synthesize GH with 1.5 mg/ml GO and 41 mmol/L of hydrazine showed that it was unsuccessful [30]. In this work a series of control experiments were performed to identify if a monolith could be assembled for specific values of GO concentration and diamine equivalents. It was evidenced that for optimized concentrations of 5 mg/ml GO and 3.7  $\mu\text{l}$  hydrazine monohydrate for 1 mg of GO respectively, a GH-HD monolith could be successfully formed (Details in SI). This finding certainly differs from what was observed in the literature. This can be explained by the higher GO concentration used in this work which promotes enhanced cross-linking between the GO sheets and gel formation [24]. GH-ED and GH-DB were also synthesized using these optimized parameters to allow clear physical and electrochemical property comparisons of the gels. The physical and chemical properties of GHs were characterized by FT-IR, TGA, XRD, XPS and conductivity measurements. SEM and BET analysis were performed to analyse the expected 3D assembly of the systems.

Fig. 1a shows the comparison of the FT-IR spectra recorded for graphene oxide and each of the gels assembled. The GO FT-IR spectra displays intense adsorption peaks at ~3400, 1728 and 1620  $\text{cm}^{-1}$  corresponding respectively to OH, C=O and C=C stretching modes which is in accordance with the high degree of oxidation of the starting material. Upon gel assembly with diamines, the broad and intense band at 3700–3200  $\text{cm}^{-1}$  is replaced



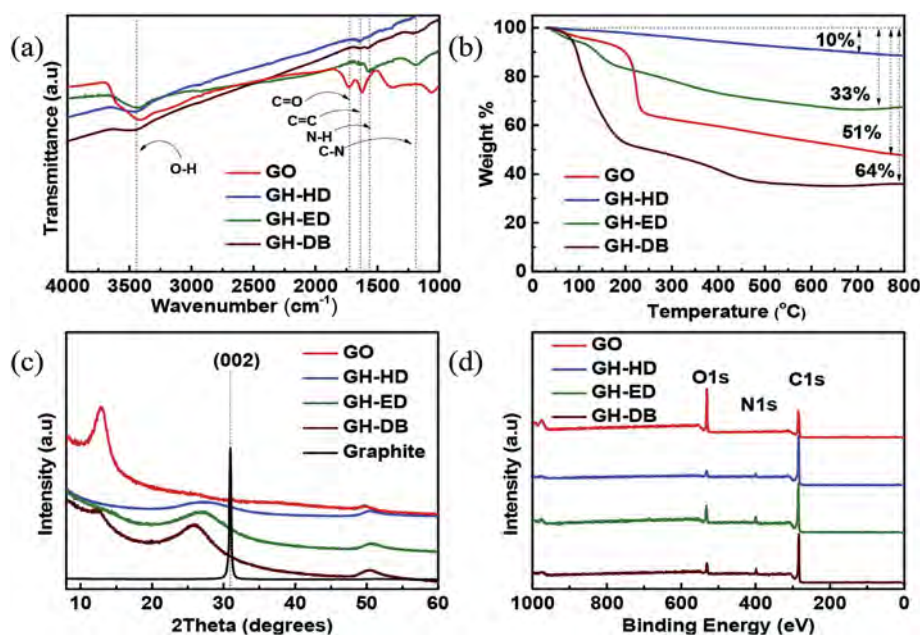


Fig. 1. (a) FT-IR spectra from the raw data, (b) TGA response under N<sub>2</sub> atmosphere, (c) XRD patterns and (d) XPS survey scans of GO and GHs.

by a relatively weak band at  $3400\text{ cm}^{-1}$ . The carbonyl signature at  $1728\text{ cm}^{-1}$  disappears while two new bands assigned to N-H of primary amines and aliphatic C-N at  $1568$  and  $1200\text{ cm}^{-1}$  respectively appear [25]. These modifications in spectra upon gel assembly can be explained by the reduction of oxygen containing function (chemical reduction) and by the diamine reaction with GO. While GH-ED and GH-DB show presence of primary amine from respective diamines with intense bands at  $1568\text{ cm}^{-1}$ , this band is much less intense for GH-HD suggesting that the gel formation mechanism with hydrazine could be different with other longer diamines.

Thermal degradation responses of GO and GHs were analyzed with TGA analysis (Fig. 1b). GO thermogram shows a typical two step degradation profile corresponding to loss of moisture at around  $100\text{ }^{\circ}\text{C}$  and decomposition of labile oxygen functionalities at  $\sim 220\text{ }^{\circ}\text{C}$  [38]. The synthesized gels show varied decomposition profiles depending on the nature of the diamine. On one hand, GH-ED and GH-DB show a gradual weight loss from  $180$  to  $350\text{ }^{\circ}\text{C}$ , similar to that of GO. This loss is explained by the presence of residual oxygen functionalities in these gels. Further, a significant weight loss could be noted around the boiling points of respective diamines ( $116$  and  $158\text{ }^{\circ}\text{C}$ ) suggesting the removal of labile diamines. From these thermograms it can be deduced that these gels are not fully reduced and that the reaction with ethylenediamine and diaminobutane successfully occurred. On the other hand, GH-HD thermogram does not indicate any significant weight loss throughout the heating range indicating lack of any labile diamine or oxygen functionalities. Thus, GH-HD demonstrates a high degree of reduction and a graphite-like thermal behaviour. As hinted by the IR study, the lack of amine loss in this gel highlights a different gel formation mechanism when longer diamines were used.

Fig. 1c displays the XRD patterns of GO and freeze dried gels. The pattern for GO depicts a relatively sharp peak at  $2\theta = 12.9^{\circ}$  corresponding to  $7.94\text{ \AA}$  of inter-layer spacing indicating high oxidation of the starting material. The synthesized GH-HD exhibits a broad peak around  $2\theta = 27.5^{\circ}$ , corresponding to the graphitic (002) orientation and an inter-graphene sheet distance of  $3.76\text{ \AA}$ . This value is very close to that of graphite itself ( $3.36\text{ \AA}$ ), evidencing a high degree of reduction of GH-HD. GH-ED and GH-DB

diffractograms display a (002) peak shifted very slightly to lower  $2\theta$  corresponding to interlayer spacing of  $3.82$  and  $4.01\text{ \AA}$  respectively. The gel formation with diamines results in removal of oxygen functional groups from the surface of GO sheets and thus partially restores the stacking as evidenced by the (002) peak shift. Among the three diamines, GH-HD shows a near graphite-like behaviour with an inter-layer spacing of  $3.76\text{ \AA}$  highlighting better degree of reduction than the other gels. Notably, GH-DB shows a pattern with a remaining GO peak around  $13^{\circ}$ .

Further, XPS was performed to analyse the surface chemical composition of GO and GHs. Fig. 1d shows survey spectra of different samples with presence of the same elements i.e. C, O and N. It is visible that depending on the samples the relative elemental concentrations vary. For example, on the GO spectra, the intensity of the O peak is higher than that of the C peak, whereas for the gels this ratio is inverted and the C peak intensity becomes higher. This evolution shows that GO is highly oxidized compared to the gels that all show a spectra indicative of a sample reduction. It is also visible that upon gel formation an additional N 1s peak appeared at  $\sim 399\text{ eV}$  giving evidence of a reaction between graphene and the diamine used for the gel structuration.

To compare the samples further, HR XPS spectra were recorded on C, O and N for each sample. As can be seen on Fig. 2a, after deconvolution, the high resolution C1s core-level spectra of GO shows four characteristic peaks at  $284.6$ ,  $285.9$ ,  $286.5$  and  $288.3\text{ eV}$  corresponding to C=C/C-C, C-OH, epoxy/alkoxy and carbonyl groups respectively [8]. For the synthesized gels, the C1s HR XPS spectra display significant decrease in the intensities of the signals arising from C in an oxidized environment (C=O, C-OH, O-C-O) and a new peak attributed to C-N bond appears at  $285.6\text{ eV}$  (Fig. 2b for GH-HD and Fig. S3 for all GHs) [25]. These findings confirm the removal of oxygen groups upon the conversion of GO to GHs due to chemical reduction and assert the reaction between GO and the diamine structuring agent. Further, restoration of the conjugation is also typically seen through  $\pi-\pi^*$  signal that occurs beyond  $290\text{ eV}$ . Such a signal could be clearly spotted in GH-HD again confirming the reduction of GO.

The reactivity between GO and the diamine structuring agent was further addressed by observing the N1s HR XPS spectra for

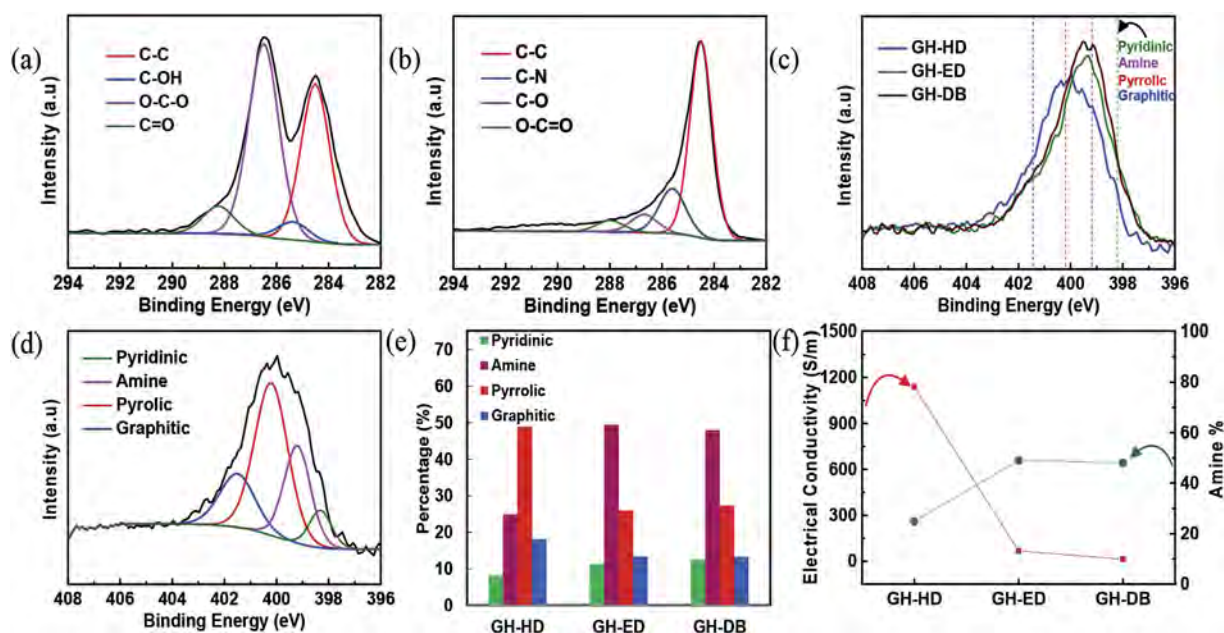


**Fig. 2.** C 1s XPS spectra of (a) GO and (b) GH-HD deconvoluted into components; (c) overlay of N 1s XPS spectra of the synthesized gels; (d) N 1s XPS spectra of GH-HD deconvoluted into components; (e) histogram showing the percentages of different N environments in the gels; (f) electrical conductivities of the gels shown with corresponding amine contents from XPS analysis.

various gels (Fig. 2c). The N1s signal for GH-HD is centred at higher binding energy of ~400 eV compared to (~399 eV) of GH-ED and GH-DB, showing variation in N environment. Furthermore, the N atomic concentration in GH-HD (4%) is lower than that for both GH-ED and GH-DB (~6%). Based on reference studies, the N 1s spectra was deconvoluted into pyridinic (398.2 eV), amine (399.2 eV), pyrrolic (400.2 eV) and graphitic (401.5 eV) components (Fig. 2d for GH-HD and Figs. S4 and S5 for all GHs) [25,29]. As evoked in the literature, these components arise from different types of Ns resulting from various possible mechanisms: the amines react covalently with the GO to form amine linkages on graphene sheets and intramolecular rearrangements with these amine linkages can cause insertion of pyridinic/pyrrolic/graphitic components into the graphene sheet [29]. An analysis of the relative intensities of all N components in the three gels is displayed in Fig. 2e. Approximately, 50% the nitrogen present in GH-ED and GH-DB corresponds to amine whereas only 25% corresponds to amine N in GH-HD. For GH-HD the main N component is pyrrolic. This differentiation may arise from different gel formation mechanisms between GO and hydrazine and GO and ED or DB. As an extension, GH-HD, even with lower N content, could present different material properties compared to GH-ED and GH-DB. For example, it is known that addition of graphitic nitrogen into graphene materials improves the electrical conductivity and presence of pyridinic nitrogen and pyrrolic nitrogen under basic conditions boost electrochemical capacitances [29,39].

Conventionally C/O ratios are analyzed as a measure of the degree of reduction of graphene materials [28]. However, carbons coming from the diaminobutane and ethylenediamine alkyl chains are added into the C content, hence, the C/O ratios obtained herein should be interpreted with caution. The obtained elemental compositions and C/O ratios of the gels are listed in Table 1. GH-HD, GH-ED and GH-DB show C/O ratios of 16.7, 7.1 and 10.7 respectively while GO demonstrates 2.6. These values further demonstrate the reduction of GO during gel formation with diamines. The C/O ratio observed for GH-HD here is greatest among the hydrazine reduction of the GO [8,9]. Repeated experiments confirm this value and

**Table 1**

Elemental composition and C/O ratios obtained from XPS, electrical conductivity ( $\sigma$ ) and discharge capacitances in F/g (Cwt) at different rates of GHs.

	C (%)	O (%)	N (%)	C/O	$\sigma$ (S/m)	C <sub>wt</sub> (F/g) at 0.5 A/g	C <sub>wt</sub> (F/g) at 100 A/g
GH-HD	90.4	5.4	4.2	16.7	1141	190	123
GH-ED	82.4	10.7	6.8	7.1	68	152	51
GH-DB	85.4	8.5	6.2	10.7	14	136	32

investigations are under way to clearly understand the merits of the current procedure over previous reduction protocols. Furthermore, the values obtained for GH-DB and GH-ED may not be a correct representation of the order of degree of reduction as greater number of alkyl carbons are added into GH-DB than GH-ED.

Electrical conductivity measurements were performed on each freeze-dried gel. From Fig. 2f, it is clear that GH-HD has nearly two fold greater conductivity (1141 S/m) compared to that of GH-ED (68 S/m) and GH-DB (14 S/m) indicating a higher reduction extent for GH-HD. Scanning electron microscopic images (Fig. 3) show that well developed extensive 3D porous networks are achieved for the gels. GH-HD is characterized by macropores diameters of several micrometres (Fig. 3a and b); whereas GH-ED and GH-DB have smaller pore volumes than GH-HD with pore diameters in sub micrometre range. Interestingly, GH-ED has larger pores than GH-DB as also seen in an earlier study of diamines with different chain lengths [23]. The specific surface areas for the gels were obtained through methylene blue (MB) dye adsorption studies. MB adsorption is extensively used to quantify the solvated surface area of a material in which any possible restacking of graphene layers is prevented by avoiding freeze drying technique [33,34,40]. GH-HD shows high specific surface area (SSA) of 1433 m<sup>2</sup>/g whereas GH-ED and GH-DB have 677 and 335 m<sup>2</sup>/g respectively. GH-HD demonstrates a porous morphology (Fig. 3a and b) that is similar to the hydrothermally synthesized gels which were found to have a SSA of 1030 and 1560 m<sup>2</sup>/g [33]. On the other hand, despite lyophilisation propensity to reduce the SSA through graphene layer restacking,

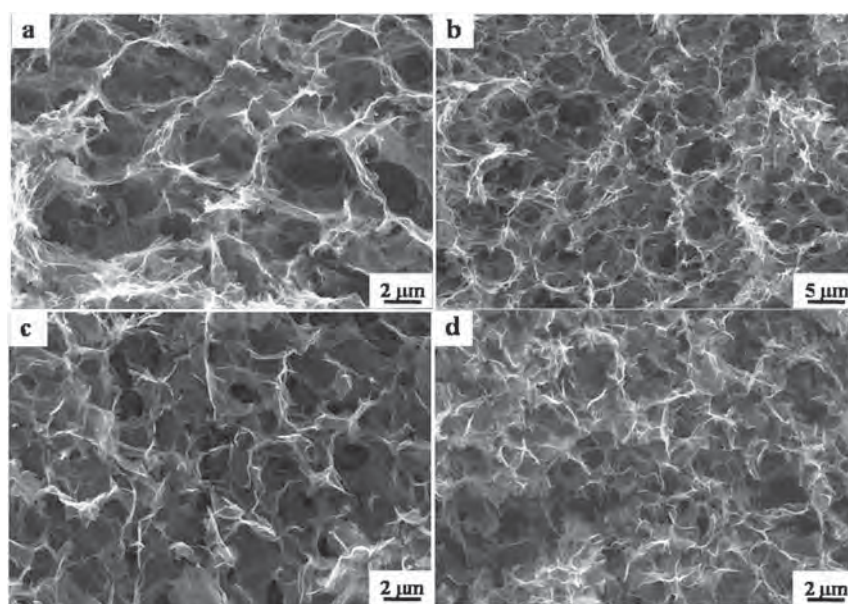


**Fig. 3.** Scanning electron microscopy images of the 3D frameworks in (a & b) GH-HD, (c) GH-ED and (d) GH-DB.

BET surface area of fully freeze-dried samples can be used to double-check this SSA difference between GH-HD and GH-ED or GH-DB, and also to compare these samples to other monoliths described in the literature. For GH-HD a  $130 \text{ m}^2/\text{g}$  SSA with a mean pore size of 25 nm is determined while for GH-ED and GH-DB the SSA are respectively 85 and  $80 \text{ m}^2/\text{g}$  with mean pore sizes of 17 and 13 nm (Fig. S6). Hence the trend obtained with MB adsorption is also observed here confirming that GH-HD monolith presents a higher surface area. It is noteworthy that the PSD also shows that GH-HD displays macroporosity as evidenced in SEM. For GH-ED gel that can be directly compared to literature data, the SSA obtained is half lower than what was described earlier [24]; however both data remain in the same range and this difference can be explained by variation in ethylenediamine concentration used leading to different graphene assembly structures. When compared to the precursor of holey graphene foam obtained by the hydrothermal route, GH-HD displays a lower SSA; however despite being prepared following different methods and using different initial GO concentration, both SSA remain in the same magnitude range [33].

Again this morphological characterization tend to prove that while the three structuring agent are diamines, they do not react identically with GO leading to GH with different properties (Proposed reaction mechanisms in ESI). As evoked before, gel formation with hydrazine occurs mainly through reduction of oxygenated functionalities on the GO sheets; this high reduction degree is confirmed with XPS, TGA and conductivity measurements. In this case the reduced graphene oxide sheets cross-link through  $\pi$ - $\pi$  stacking resulting in 3D framework with entrapped water [12]. For ethylenediamine and diaminobutane structuring agents, the nature of the reaction is more covalent and the amine functions will react with C in an oxidized environment. The reductive power of these two amines compared to hydrazine are lower explaining that this reduction based gel formation path is not favoured. In this case, the 3D assembly is triggered by covalent cross-linking leading to structures with smaller pore volumes. This gel comparison therefore shows that in a one step process by selecting a diamine that remains short and display a high reductive power, a gel with interestingly high conductivity and porosity can be formed. It is noteworthy that the GH-HD conductivity and porosity fall in the same range than that of the further reduced hydrothermally

synthesized gel [12].

### 3.1. Electrochemical studies on GHs

GHs synthesized with different diamine chain lengths were tested in a two electrode supercapacitor configuration with aqueous potassium hydroxide (6 M) as electrolyte. Since the gels were prepared in aqueous media, they enable facile assembly into aqueous electrolyte without much processing. Slices of gels were assembled symmetrically without any conductive additives or binding agents. CV, galvanostatic charge-discharge at different current densities and EIS were performed to evaluate the electrochemical performances.

CV curves were obtained in the potential range of 0–1 V at relatively low and high scan rates of 100 mV/s and 1000 mV/s. At a lower scan rate all three gels show rectangular curves with little deformation suggesting mainly electrochemical double layer capacitance (EDLC) mechanism with good charge propagation at the electrode-electrolyte interface (Fig. 4a). Upon increasing the scan rate from 100 mV/s to 1000 mV/s, the CV curves of GH-HD and GH-ED retain a nearly rectangular shape while that of GH-DB distorts into narrow and oblique rectangle (Fig. 4b). Charge storage mechanism which involves adsorption-desorption of the ionic species at the electrode surfaces depends on the time scales of the electrochemical processes. High scan rates or charge-discharge current densities may not allow sufficient time for double layer formation and thus could result in such resistive behaviour. Notably, GH-HD offers greater current densities compared to the other two gels at both scan rates. These results suggest better electrolyte ion transport characteristics and higher ion accessible surface areas in GH-HD.

The slight deformation in the CVs at 100 mV/s could possibly be due to redox activity of the nitrogen and oxygen content in the synthesized gels. CVs at a low scan rate of 10 mV/s were performed and indeed a greater deformation could be seen in all the gels (Fig. S8). Three electrodes configuration allows to study the individual electrode response and could give additional information over the two-electrode measurements. Hence, CVs were obtained at 10 and 100 mV/s scan rates for all the gels in the voltage range of –0.9 V to 0.1 V vs. standard calomel electrode (Fig. S9). 3-



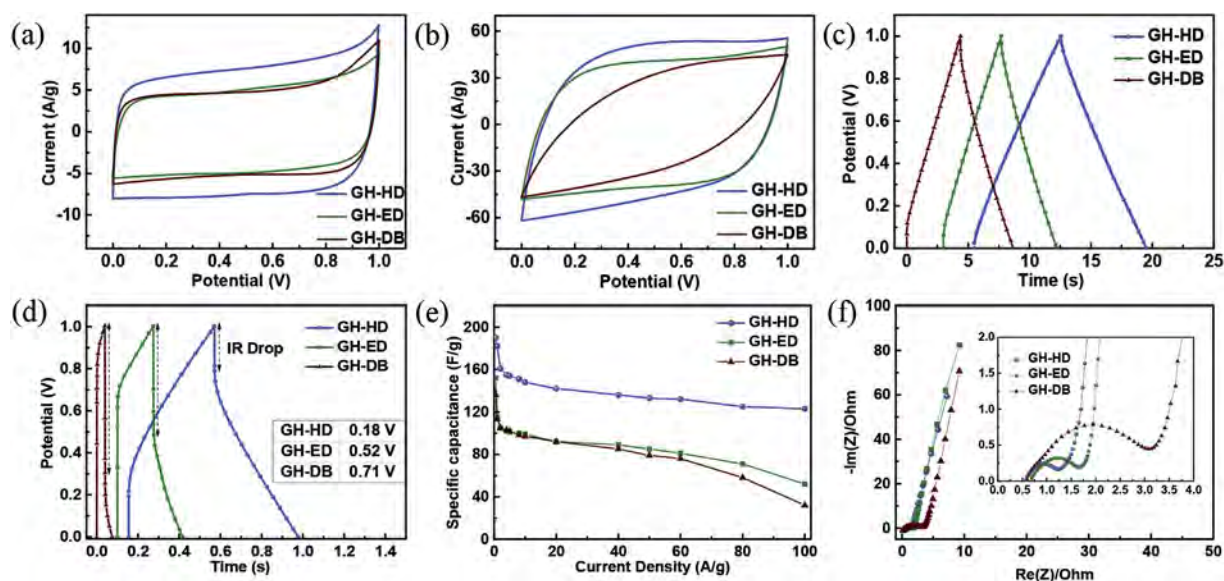


**Fig. 4.** Cyclic voltammograms of gels obtained at scan rates of (a) 100 mV/s and (b) 1000 mV/s in the voltage range of 0–1 V; galvanostatic charge-discharge voltage profiles of the gels obtained at current densities of (c) 10 A/g and (d) 100 A/g; (e) rate capability and (f) Nyquist plot obtained from frequency response of the gels from 400 kHz to 40 mHz. Inset shows a magnified plot with frequency response at high frequencies.

electrodes CVs of the three gels show similarly slightly distorted rectangular shape and confirm the contribution of pseudo capacitance from N and O functionalities [29]. Among the three gels, GH-HD demonstrates more intense redox peaks (–0.6 V vs. SCE) than GH-ED and GH-DB. Good electrical conductivity of the material for better electron transport to and from the redox active sites and higher redox active N content explain the more intense pseudo capacitance peaks in the case of GH-HD. A table (Table S1.) comparing the three-electrode electrochemical performance of GH-HD with literature can be found in the ESI.

Galvanostatic charge-discharge cycling of gels was performed at high current densities of 10 A/g and 100 A/g. At 10 A/g, symmetrical charge-discharge curves (Fig. 4c) could be seen for all the gels in agreement with the major EDLC behaviour observed in the CV curves. GH-ED and GH-DB suffer from a slight internal resistance (IR) drop of 0.04 V and 0.06 V respectively, whereas GH-HD has no drop in voltage. The voltage drop caused by IR of the electrodes is more significant when cycling is done at high current densities. When cycled at a very high current density of 100 A/g, GH-ED and GH-DB show an asymmetric voltage profile with huge IR drops of 0.52 V and 0.71 V respectively (Fig. 4d). Similar IR drops were observed in literature when cycled at high current density of 100 A/g [28]. GH-HD retains a nearly symmetric behaviour with an IR drop value of 0.18 V. This can be understood from the high electrical conductivity of GH-HD (1141 S/m) as compared to GH-ED (68 S/m) and GH-DB (14 S/m). High electrical conductivity of GH-HD ensures lower IR drops and energy loss as heat, enabling better rate performance.

Gravimetric capacitances of cycling at 0.5 A/g and 100 A/g are obtained by calculating the slope of the discharge curves and are listed in Table 1. Fig. 4e shows the power capability of GHs in a range of current densities from 0.5 A/g to 100 A/g. GH-HD delivers 190 F/g at 0.5 A/g, which is similar to that of hydrothermally synthesized gels (200 F/g at 0.3 A/g). GH-ED and GH-DB deliver capacitances of 152 F/g and 136 F/g under same conditions. At a high current density of 100 A/g, GH-HD offers discharge capacitance of 123 F/g whereas GH-ED and GH-DB yield poor discharge capacitances of 51 F/g and 32 F/g respectively. The superior performance of GH-HD compared to GH-ED and GH-DB is attributed to multiple

factors. Firstly, GH-HD has a greater wet-state surface area of 1433 m<sup>2</sup>/g whereas GH-ED and GH-DB have 677 and 335 m<sup>2</sup>/g respectively. Also, the excellent electrical conductivity of GH-HD enables fast charge transfer at the electrode-electrolyte interface and allows better rate performance. The extensive 3D networks with large pore volumes facilitate fast ion transfer to the electrode interface. Moreover, the lower percentage of amine N in GH-HD than other gels results in greater pseudo capacitive contribution by redox active N components. As a result of increased electrolyte access to electrode surface, higher conductivity and greater pseudo capacitive contributions, enhanced electrochemical capacitances are observed in GH-HD.

Charge and ion-transfers inside the highly conductive and porous GH-HD have been shown to be at the origin of its good SC electrochemical performances. An EIS study has therefore been performed to analyse these factors more directly Fig. 4f. Indeed this technique offers the frequency response from 400 kHz to 40 mHz yielding a Nyquist plot with real and imaginary components of impedance X and Y axes respectively, and each region of the plot will give direct evidence of a specific process. First, an arc at high frequency region is ascribed to charge transfer resistance, the 45° slope of Warburg impedance in intermediate frequency range is related to ion diffusion and finally the nearly vertical line at higher frequency shows the capacitive behaviour of the system. GH-HD exhibits the smallest semi-circle diameter and its charge-transfer resistance ( $R_{CT}$ ) was deduced to be 0.62  $\Omega$  compared to 1  $\Omega$  for GH-ED and 2.46  $\Omega$  of GH-DB. Also the shorter Warburg impedance region for GH-HD indicates the most efficient ion transfer among the three gels. These two findings corroborate the positive impact of the superior electrical conductivity and porosity of GH-HD on electrode charge-transfer and ion-diffusion.

The electrochemical data recorded in this work (GH-HD and GH-ED) are positioned on a Ragone plot with comparative values of GHs prepared through various reduction methods in the literature (Fig. 5a) [41,42]. When cycled at a high current density of 100 A/g, with a sub-second discharge time of 0.4s, GH-HD offers a high power density of 38 kW/kg while delivering an energy density of 4.3 Wh/kg. The observed values are on par with the best reported energy and power densities in aqueous electrolytes. GH-HD

outperforms GHs synthesized through reduction of GO by hydrothermal treatment [12], thermal treatment [41] and L-glutathione [42]. Also, GH-HD performs better than both GH-ED and ethylenediamine assisted gel obtained with an extra step of hydrazine reduction as reported in the literature [24]. Table S2 compares the electrochemical performance of GH-HD with various reports on carbon materials for supercapacitors in the literature. The electrochemical performances achieved with GH-HD are high and fall in the range of values obtained for hydrothermal gel further reduced by hydrazine, which display a power density of 30 kW/kg and energy density of 5.7 Wh/kg at 100 A/g [28]. Current efforts are devoted towards achieving higher energy densities by benefiting from large stable voltage ranges of non-aqueous electrolytes. Preliminary results using 1 M Tetraethylammonium tetrafluoroborate/Acetonitrile (TEABF<sub>4</sub>/ACN) as the electrolyte also show better performance of GH-HD among the synthesized gels (Fig. S10).

The cycling study showed full capacity retention with GH-HD after 5000 cycles of charge-discharge at a low current density of 2 A/g (Fig. S11). Recorded at a higher rate of 10 A/g, 93% retention of discharge capacitance was obtained after 2000 cycles (Fig. 5b). The observed cyclic stability is better than the 92% capacitance retention reported at an intermediate 4 A/g after 2000 cycles for the hydrazine-reduced hydrothermal gel. These results further demonstrate the merits of GH-HD which is obtained by a simple one-step process involving equivalent amount of hydrazine.

Further, upon inspecting the Ragone plot, an initial report on gaseous-hydrazine reduced CMG could be seen to deliver a high energy density 7 Wh/kg with a power density of 0.5 kW/kg at 0.1 A/g [43]. The rate performance of this CMG was, unfortunately, not evaluated at higher current densities. The synthesized CMG was characterized with high electrical conductivity and stacked morphology of the reduced graphene oxide sheets. We believed that a study of the electrochemical performance of this highly conducting CMG compared to GH-HD would help us critically analyse the implications of 3D porous networks in SC

performances. For this purpose, we performed a controlled study by synthesizing CMG under similar reaction conditions as for GH-HD with continuous stirring (procedures in ESI). Four probe measurements showed an improved electrical conductivity of 1832 S/m compared to GH-HD (1141 S/m) as can be understood by greater extent of reduction under homogenized reaction media. CV of CMG shows an ideal EDLC behaviour at 100 mV/s but distorts into an oblique shape at a high scan rate of 1000 mV/s (Fig. S12). Power capability study from 0.5 A/g to 100 A/g shows a similar performance of CMG to that of GH-HD at lower rates but a huge drop is noticed with increasing currents (Fig. 5c). Despite being a better electrical conductor, CMG shows poorer electrochemical performance than GH-HD at higher currents. This can be explained by the difference in porosity characteristics (Fig. S7). While, CMG performs well at lower current densities, the compact porous structure prevents seamless ion transport at higher densities. The extensive porous network in GH-HD enables excellent ion accessibility to the electrode-electrolyte interface even at higher currents. From these observations, it can be concluded that, 3D interconnected porous network, along with good electrical conductivity, is an equally important factor in enabling a high power capability of a SCs.

Finally, considering the importance of good volumetric capacitances for SC applications with limited space, we synthesized a dense GH-HD gel by following a simple drying procedure. After gel assembly with hydrazine, GH-HD was densified from a packing density of 0.58 g/cm<sup>3</sup> to 1.56 g/cm<sup>3</sup> by drying it under ambient conditions. The gradual removal of water molecules from the inter layer spaces shrinks the gel to nearly a tenth of its original size. Fig. 5d shows the cyclic stability of GH-HD and its densified counterpart (GH-HD-AD) at a current density of 2 A/g. The volumetric capacitances of GH-HD could be noted to increase by a factor of two. GH-HD-AD delivers gravimetric and volumetric discharge capacitances of 130 F/g and 200 F/cm<sup>3</sup> respectively at a high current density of 2 A/g.

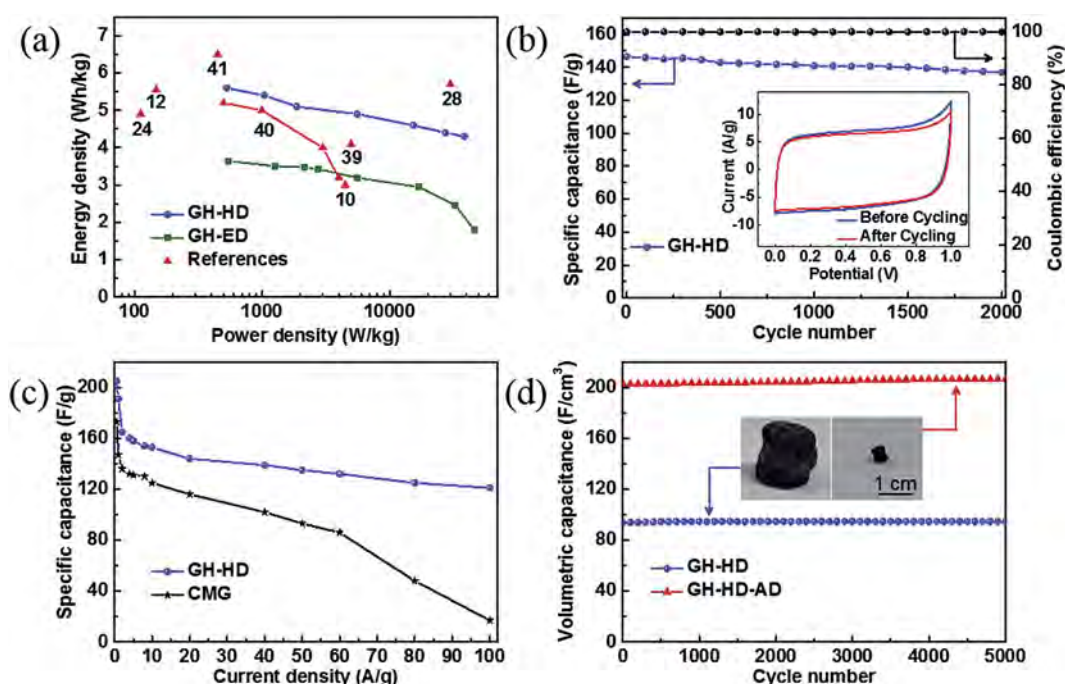


**Fig. 5.** (a) Ragone plot showing a comparison of energy and power densities of GH-HD and GH-ED with references from literature based on graphene based materials obtained by various reduction techniques; (b) cyclic stability of GH-HD obtained at high current density of 10 A/g; Inset shows CVs at a scan rate of 100 mV/s for GH-HD before the 1st and after the 2000<sup>th</sup> charge-discharge cycle; (c) rate capability of GH-HD and CMG; (d) cyclic stability of GH-HD and densified GH-HD-AD obtained at a current density of 2 A/g.

## 4. Conclusions

GH-HD was prepared as a highly conducting monolith using a simple one-step synthesis process. An optimization study of the reaction conditions enabled such a hydrogel assembly. GH-ED and GH-DB based on longer diamines were also synthesized to analyse different mechanisms and their implications. Hydrazine, being a strong reducing agent, promotes gel formation via assembly of reduced GO through non-covalent interactions such as  $\pi$  -  $\pi$  interactions. When tested in aqueous SC, GH-HD with a low charge transfer resistance of 0.62  $\Omega$  and excellent 3D macroporous network, offered high rate performance. An excellent cycling stability with 93% capacitance retention was noted after cycling for 2000 cycles at a high current density of 10 A/g and full capacitance was observed when cycled at lower rate of 2 A/g over 5000 cycles. Furthermore, at a very high current density of 100 A/g discharge capacitance of 123 F/g could be achieved. Extensive 3D porous networks along with high electrical conductivity were evidenced as the major factors behind such performances. The control study performed in this work to understand the interplay between electrical conductivity and porosity in electrochemical performances allows us to design superior materials for SCs. The simple one-step synthesis procedure under atmospheric conditions to obtain highly reduced GHs could enable the development of low cost and high power performance SCs.

## Acknowledgements

The authors would like to acknowledge the French ANR program (SUGGEST ANR project - ANR-15-CE05-0022) as well as CEA for their financial support. This work has been performed with the use of the Hybriden facility at CEA-Grenoble (France). The access to mutualized equipment and PFNC Nano characterization Minattec platforms was appreciated by the authors. S. Pouget is thanked for her help in XRD training, E. Dubard for her assistance with TGA and N. Pauc for conductivity measurements training. The authors are obliged to G. Bidan, O. Crosnier, P. Simon and P.-L. Taberna for fruitful discussions.

## Appendix A. Supplementary data

Supplementary data related to this article can be found at <http://dx.doi.org/10.1016/j.jpowsour.2017.06.033>.

## References

- [1] G. Wang, L. Zhang, J. Zhang, A review of electrode materials for electrochemical supercapacitors, *Chem. Soc. Rev.* 41 (2012) 797–828.
- [2] P. Simon, Y. Gogotsi, Materials for electrochemical capacitors, *Nat. Mater.* 7 (2008) 845–854.
- [3] A. Burke, R&D Considerations for the performance and application of electrochemical capacitors, *Electrochim. Acta* 53 (2007) 1083–1091.
- [4] J.R. Miller, P. Simon, Electrochemical capacitors for energy management, *Science* 321 (2008) 651–652.
- [5] L.L. Zhang, X.S. Zhao, Carbon-based materials as supercapacitor electrodes, *Chem. Soc. Rev.* 38 (2009) 2520–2531.
- [6] Y. Zhu, S. Murali, W. Cai, X. Li, J.W. Suk, J.R. Potts, R.S. Ruoff, Graphene and graphene oxide: synthesis, properties, and applications, *Adv. Mater.* 22 (2010) 3906–3924.
- [7] J. Xia, F. Chen, J. Li, N. Tao, Measurement of the quantum capacitance of graphene, *Nat. Nano* 4 (2009) 505–509.
- [8] S. Stankovich, D.A. Dikin, R.D. Piner, K.A. Kohlhaas, A. Kleinhammes, Y. Jia, Y. Wu, S.T. Nguyen, R.S. Ruoff, Synthesis of graphene-based nanosheets via chemical reduction of exfoliated graphite oxide, *Carbon* 45 (2007) 1558–1565.
- [9] D. Li, M.B. Muller, S. Gilje, R.B. Kaner, G.G. Wallace, Processable aqueous dispersions of graphene nanosheets, *Nat. Nano* 3 (2008) 101–105.
- [10] M.D. Stoller, S. Park, Y. Zhu, J. An, R.S. Ruoff, Graphene-based ultracapacitors, *Nano Lett.* 8 (2008) 3498–3502.
- [11] H. Bai, C. Li, X. Wang, G.A. Shi, A pH-sensitive graphene oxide composite hydrogel, *Chem. Commun.* 46 (2010) 2376–2378.
- [12] Y. Xu, K. Sheng, C. Li, G. Shi, Self-assembled graphene hydrogel via a one-step hydrothermal process, *ACS Nano* 4 (2010) 4324–4330.
- [13] Y. Xu, Q. Wu, Y. Sun, H. Bai, G. Shi, Three-dimensional self-assembly of graphene oxide and DNA into multifunctional hydrogels, *ACS Nano* 4 (2010) 7358–7362.
- [14] C. Li, G. Shi, Functional gels based on chemically modified graphenes, *Adv. Mater.* 26 (2014) 3992–4012.
- [15] H. Bai, C. Li, X. Wang, G. Shi, On the gelation of graphene oxide, *J. Phys. Chem. C* 115 (2011) 5545–5551.
- [16] P.M. Sudeep, T.N. Narayanan, A. Ganesan, M.M. Shaajumon, H. Yang, S. Ozden, P.K. Patra, M. Pasquali, R. Vajtai, S. Ganguli, A.K. Roy, M.R. Anantharaman, P.M. Ajayan, Covalently interconnected three-dimensional graphene oxide solids, *ACS Nano* 7 (2013) 7034–7040.
- [17] Z. Lei, J. Zhang, L.L. Zhang, N.A. Kumar, X.S. Zhao, Functionalization of chemically derived graphene for improving its electrocapacitive energy storage properties, *Energy Environ. Sci.* 9 (2016) 1891–1930.
- [18] Y. Chen, L. Chen, H. Bai, L. Li, Graphene oxide-chitosan composite hydrogels as broad-spectrum adsorbents for water purification, *J. Mat. Chem. A* 1 (2013) 1992–2001.
- [19] S. Park, K.-S. Lee, G. Bozoklu, W. Cai, S.T. Nguyen, R.S. Ruoff, Graphene oxide papers modified by divalent ions-enhancing mechanical properties via chemical cross-linking, *ACS Nano* 2 (2008) 572–578.
- [20] B. Adhikari, A. Biswas, A. Banerjee, Graphene oxide-based hydrogels to make metal nanoparticle-containing reduced graphene oxide-based functional hybrid hydrogels, *ACS Appl. Mat. Interfaces* 4 (2012) 5472–5482.
- [21] B. Adhikari, A. Biswas, A. Banerjee, Graphene oxide-based supramolecular hydrogels for making nanohybrid systems with Au nanoparticles, *Langmuir* 28 (2012) 1460–1469.
- [22] Y. Xu, G. Shi, X. Duan, Self-assembled three-dimensional graphene macrostructures: synthesis and applications in supercapacitors, *Acc. Chem. Res.* 48 (2015) 1666–1675.
- [23] P. Chen, J.-J. Yang, S.-S. Li, Z. Wang, T.-Y. Xiao, Y.-H. Qian, S.-H. Yu, Hydrothermal synthesis of macroscopic nitrogen-doped graphene hydrogels for ultrafast supercapacitor, *Nano Energy* 2 (2013) 249–256.
- [24] V.H. Luan, H.N. Tien, L.T. Hoa, N.T.M. Hien, E.-S. Oh, J. Chung, E.J. Kim, W.M. Choi, B.-S. Kong, S.H. Hur, Synthesis of a highly conductive and large surface area graphene oxide hydrogel and its use in a supercapacitor, *J. Mat. Chem. A* 1 (2013) 208–211.
- [25] H. Hu, Z. Zhao, W. Wan, Y. Gogotsi, J. Qiu, Ultralight and highly compressible aerogels, *Adv. Mater.* 25 (2013) 2219–2223.
- [26] J. Che, L. Shen, Y. Xiao, A new approach to fabricate graphene nanosheets in organic medium: combination of reduction and dispersion, *J. Mat. Chem.* 20 (2010) 1722–1727.
- [27] X. Zhang, Z. Sui, B. Xu, S. Yue, Y. Luo, W. Zhan, B. Liu, Mechanically strong and highly conductive graphene aerogel and its use as electrodes for electrochemical power sources, *J. Mat. Chem.* 21 (2011) 6494–6497.
- [28] L. Zhang, G. Shi, Preparation of highly conductive graphene hydrogels for fabricating supercapacitors with high rate capability, *J. Phys. Chem. C* 115 (2011) 17206–17212.
- [29] H.-L. Guo, P. Su, X. Kang, S.-K. Ning, Synthesis and characterization of nitrogen-doped graphene hydrogels by hydrothermal route with urea as reducing-doping agents, *J. Mat. Chem. A* 1 (2013) 2248–2255.
- [30] W. Chen, L. Yan, In situ self-assembly of mild chemical reduction graphene for three-dimensional architectures, *Nanoscale* 3 (2011) 3132–3137.
- [31] Y. Tao, X. Xie, W. Lu, D.-M. Tang, D. Kong, Z. Huang, H. Nishihara, T. Ishii, B. Li, D. Golberg, F. Kang, T. Kyotani, Q.-H. Yang, Towards ultrahigh volumetric capacitance: graphene derived highly dense but porous carbons for supercapacitors, *Sci. Rep.* 3 (2013) 2975.
- [32] Y. Gogotsi, P. Simon, True performance metrics in electrochemical energy storage, *Science* 334 (2011) 917–918.
- [33] Y. Xu, Z. Lin, X. Zhong, X. Huang, N.O. Weiss, Y. Huang, X. Duan, Holey graphene frameworks for highly efficient capacitive energy storage, *Nat. Commun.* 5 (2014) 4554.
- [34] X. Yang, C. Cheng, Y. Wang, L. Qiu, D. Li, Liquid-mediated dense integration of graphene materials for compact capacitive energy storage, *Science* 341 (2013) 534–537.
- [35] X. Feng, N. Chen, Y. Zhang, Z. Yan, X. Liu, Y. Ma, Q. Shen, L. Wang, W. Huang, The self-assembly of shape controlled functionalized graphene-MnO<sub>2</sub> composites for application as supercapacitors, *J. Mat. Chem. A* 2 (2014) 9178–9184.
- [36] X. Feng, N. Chen, J. Zhou, Y. Li, Z. Huang, L. Zhang, Y. Ma, L. Wang, X. Yan, Facile synthesis of shape-controlled graphene-polyaniline composites for high performance supercapacitor electrode materials, *New J. Chem.* 39 (2015) 2261–2268.
- [37] W.S. Hummers, R.E. Offeman, Preparation of graphitic oxide, *J. Am. Chem. Soc.* 80 (1958) 1339.
- [38] B. Song, C. Sizemore, L. Li, X. Huang, Z. Lin, K. Moon, C.-P. Wong, Triethanolamine functionalized graphene-based composites for high performance supercapacitors, *J. Mat. Chem. A* 3 (2015) 21789–21796.
- [39] H.M. Jeong, J.W. Lee, W.H. Shin, Y.J. Choi, H.J. Shin, J.K. Kang, J.W. Choi, Nitrogen-doped graphene for high-performance ultracapacitors and the importance of nitrogen-doped sites at basal planes, *Nano Lett.* 11 (2011) 2472–2477.
- [40] C. Pelekani, V.L. Snoeyink, Competitive adsorption between atrazine and

- methylene blue on activated carbon: the importance of pore size distribution, *Carbon* 38 (2000) 1423–1436.
- [41] Q. Du, M. Zheng, L. Zhang, Y. Wang, J. Chen, L. Xue, W. Dai, G. Ji, J. Cao, Preparation of functionalized graphene sheets by a low-temperature thermal exfoliation approach and their electrochemical supercapacitive behaviors, *Electrochim. Acta* 55 (2010) 3897–3903.
- [42] H. Gao, F. Xiao, C.B. Ching, H. Duan, High performance asymmetric supercapacitor based on graphene hydrogel and nanostructured  $\text{MnO}_2$ , *ACS Appl. Mat. Interfaces* 4 (2012) 2801–2810.
- [43] Y. Wang, Z. Shi, Y. Huang, Y. Ma, C. Wang, M. Chen, Y. Chen, Supercapacitor devices based on graphene materials, *J. Phys. Chem. C* 113 (2009) 13103–13107.